
ELSEVIER

Pattern Recognition Letters 21 (2000) 1215–1223

Pattern Recognition Letters

www.elsevier.nl/locate/patrec

Quantitative measurement of changes in retinal vessel diameter in ocular fundus images

L. Pedersen [a,*], M. Grunkin [b], B. Ersbøll [a], K. Madsen [a], M. Larsen [c], N. Christoffersen [c], U. Skands [b]

[a] *Department of Mathematical Modelling, Technical University of Denmark, Building 321, DK-2800 Lyngby, Denmark*
[b] *Torsana Diabetes Diagnostics A/S, Dr. Neergaardsvej 3, DK-2970 Hørsholm, Denmark*
[c] *Herlev Hospital, University of Copenhagen, DK-2730 Herlev, Denmark*

Abstract

The change in diameter of retinal vessels as a function of increasing distance to the optic disc is believed to be indicative of the risk level of various vascular diseases such as generalised arteriosclerosis and Diabetes Mellitus. In particular, focal arteriolar narrowing (FAN) is considered related to arteriosclerosis. The aim of this work is to develop methods to provide quantitative information about the FAN status of retinal arteriolar vessel segments. We propose a method to measure the vessel diameter and changes herein along the vessel. The width or diameter measurement is based on intensity profiles orthogonal to a smoothed trace in the vessel found by Dijkstra's shortest path algorithm. The vessel diameter is calculated from the intensity profiles using two different methods to estimate profile widths. We propose a "normalised accumulated gradient" (NAG) and the coefficient of variance (CV) to estimate the FAN in a vessel segment. The NAG is designed to detect increases in the vessel diameter as the distance to the papilla increases. The performance of the methods developed is compared to the evaluation by a skilled ophthalmologist. The methods are seen to perform well.

Keywords: Image analysis; Vessel diameter measurement; Fundus images; Focal arteriolar narrowing

1. Introduction

Previously, Brinchmann-Hansen and Engvold (1986) and Brinchmann-Hansen and Heier (1986) have measured the width of the blood column in retinal vessels using microdensitometry and found that changes in the width of the blood column may be related to (pathological) changes in the vessel wall. Also, the importance of the central light reflex on retinal vessels has been investigated in detail by this group (Brinchmann-Hansen and Heier, 1986). The group uses the full width half maximum method to determine the width of a vessel.

Diabetic Retinopathy is of particular interest to many researchers and several groups attempt to quantify signs of Diabetic Retinopathy by means of image analysis. Gregson et al. (1995) and Kozousek et al. (1992) have introduced a method to detect and grade venous beading, which is "the more powerful predictor of conversion to proliferative retinopathy than any other type of retinal abnormality", reported by Early Treatment

* Corresponding author.
E-mail address: lap@imm.dtu.dk (L. Pedersen).

0167-8655/00/$ - see front matter
PII: S0167-8655(00)00084-2

Diabetic Retinopathy Study Group (1992). Beading of a vessel is repeated narrowings and widenings along the vessel and looks like sausages on a string. In the quantification of the venous beading this group proposes an alternative method to measure the vessel diameter.

In the present work, we have used both methods to estimate the vessel diameter.

Arteriosclerotic Retinopathy is a series of changes in the *retina* that are caused by arteriosclerosis. Some of these changes are hardening, attenuation (narrowing) and straightening of the retinal arterioles. Today, there is no direct method to diagnose and evaluate Arteriosclerotic Retinopathy and the progress or evolution of the disease. Clinicians use blood samples to measure cholesterol and fat contents of the blood as an indicator of the patient's risk level for generalised arteriosclerosis. Also, measurement of blood pressure is used. Still, it is difficult to assess the *accumulated effects*, since the mentioned measurements are very instant. Manifest diseases as cerebral thrombosis or coronary thrombosis are good indicators of arteriosclerosis, but when the disease has reached this state, it is very serious, and largely irreversible. At this point the vessel diameter in critical areas, is reduced to only about 20% of the original diameter. Arteriosclerosis is a systemic disease, i.e., if present in the retinal arterioles (Arteriosclerotic Retinopathy), the disease affects the entire circulatory system. This motivates for development of methods to estimate the status of arterioles in the retina. In general on the ophthalmic issues see e.g., Albert and Jakobiec (1994).

Fig. 1 shows a principal sketch of a focal arteriolar narrowing (FAN) together with an example from an arteriosclerotic patient. FAN is a focal narrowing of the arteriole and is considered to be a sign of arteriosclerosis, with the exception, that overlaying retinal nerve fibres may induce, in rare cases, optical effects that give a false impression of FAN. The evaluation of FAN is important, because of it's close relation to arteriosclerosis. This constitutes the motivation for development of methods to objectively quantify the degree of FAN.

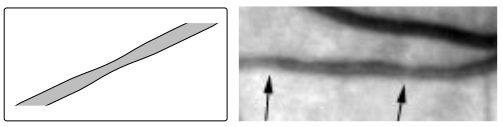

Fig. 1. Focal arteriolar narrowing in principal sketch and in arteriole segment from arteriosclerotic patient. (a) Principal sketch of arteriole segment with focal arteriolar narrowing (FAN); (b) Example of arteriole with FAN, marked with arrows, the arteriole is the bright vessel.

2. Methods

We propose the following four steps to measure the FAN in a vessel segment. Consider a vessel segment with no bifurcations or crossings. Inside the segment, the human operator has supplied two points between which the diameter will be measured.

- Dijkstra's shortest path algorithm is used to find a trace (the shortest path between the two points) inside the vessel and in its direction.
- The trace is smoothed and vessel intensity profiles are picked up, orthogonal to the trace.
- The vessel diameter is estimated as the width of the intensity profiles.
- The FAN is estimated from the vessel diameter along the vessel.

The steps are described in further detail in the sections to follow.

2.1. Dijkstra's shortest path algorithm in fundus images

Dijkstra's algorithm (Dijkstra, 1959), see e.g., Cormen et al. (1997, p. 527), can be used to find a trace between to points in a fundus image. Given two points p_1 and p_2 in the same vessel segment, the algorithm returns a shortest path between the points. Consider the grey level image as a landscape with low intensity values corresponding to low altitude and high intensity values to high altitude. The algorithm will find a path running in the bottom of the valleys because here, the intensity values are low and therefore the pixel values contribute less to the accumulated cost. The accumulated cost is simply the sum of the intensity values $I(p)$ along the path:

$$\mathscr{C}_1 = \sum_{p=p_1}^{p_2} I(p)w, \tag{1}$$

where p is the points on the path between p_1 and p_2, $w = 1$ for horizontal and vertical neighbours and $w = \sqrt{2}$ for diagonal neighbours. The trace found using the $\mathscr{C}_1$ is illustrated in Fig. 2(b).

If a neighbouring vessel is very dark (deep), the algorithm may return a shortest path, running in the neighbour vessel (see Fig. 2(c)). To prevent this, it may be desirable to use an alternative cost function, that punishes change in altitude, i.e., deviations from a level, l based on, e.g., the mean intensities in the eight neighborhood vicinities of the points p_1 and p_2. This alternative is

$$\mathscr{C}_2 = \sum_{p=p_1}^{p_2} \|I(p) - l\|w, \tag{2}$$

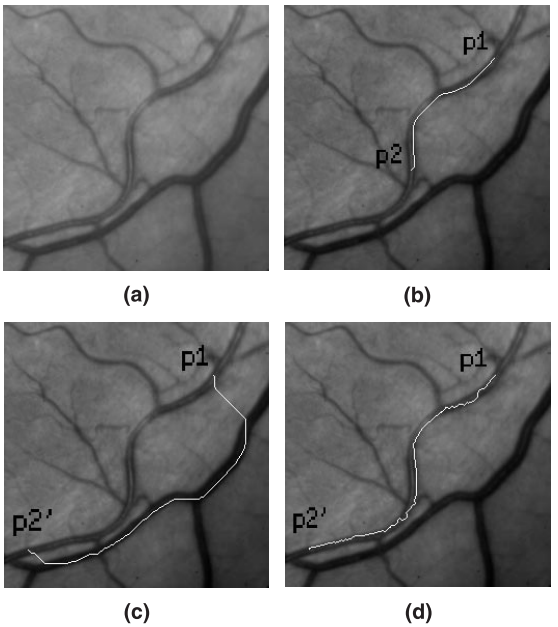

Fig. 2. The track found by using Dijkstra's shortest path algorithm on example image. (a) The original image; (b) shows the shortest path between p_1 and p_2 using cost function $\mathscr{C}_1$; (c) the end point is moved to p_2' and the algorithm finds the shortest path from p_1 to p_2' to be through the neighbouring, very dark (deep, low cost) vein using cost function $\mathscr{C}_1$; (d) the shortest path is more curly, but inside the arteriole. Here the alternative cost function $\mathscr{C}_2$ is used.

where p is the points on the path between p_1 and p_2, $w = 1$ for horizontal and vertical neighbours and $w = \sqrt{2}$ for diagonal neighbours (Fig. 2(d)).

2.2. Calculation of vessel intensity profiles

In order to assess the changes in the vessel diameter along a vessel segment, intensity profiles orthogonal to the vessel direction are computed. The trace is found using Dijkstra's algorithm and the trace coordinates are then smoothed using a 20 pixel wide averaging window. Intensity profiles, perpendicular to the trace, are obtained using bilinear interpolation. This results in an intensity profile belonging to each point in the smoothed path. Fig. 3 shows every second of the orthogonal profile lines overlaid a vessel segment. A typical intensity profile is shown in Fig. 4(a).

2.3. Vessel diameter measurement

The intensity profiles show large varieties in shape. Often, the background levels (the left and right part of the profile, i.e., the retina outside the vessel) are different and an axial reflex (AR) is often seen in the centre of the profile.

The AR is an optical phenomenon occurring as a light streak in the centre of the vessels. The importance of the presence, width and intensity of the reflex is not agreed upon.

In this work, however, we will not consider the importance of the AR but in order to measure the vessel diameter in a robust way, we must take the possible profile shapes into account, i.e., different background levels, presence of axial reflex etc. The success of the methods presented for vessel diameter measurement is highly dependent on robust estimates of the background intensity levels. This

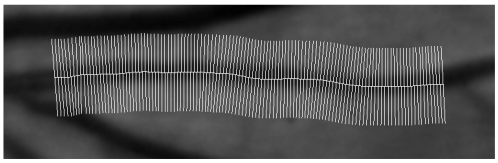

Fig. 3. Profile lines, overlaid vessel segment. The intensity profiles are "picked up" in the image along the profile lines, orthogonal to the trace.

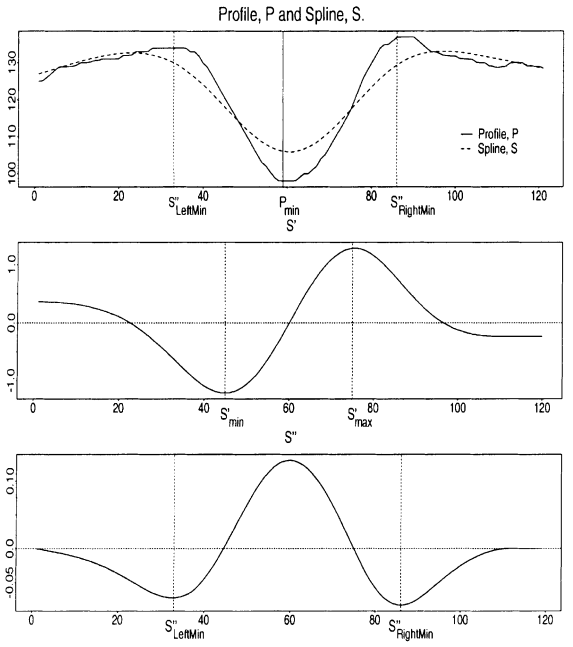

Fig. 4. (a) Typical profile with spline, S; solid, vertical line show $P_{\min}$, dotted vertical lines are S''_{LeftMin} and S''_{RightMin}. (b) First derivative of spline, S' with $S'_{\min}$ and $S'_{\max}$ as dotted vertical lines. (c) Second derivative of spline, S''; the dotted vertical lines indicate S''_{LeftMin} and S''_{RightMin}.

is the motivation for the procedure described in the Section 2.3.1.

2.3.1. Calculation of background level estimates

The profile shape is modelled using a smoothing cubic spline. From the spline and its derivatives, the locations of the background levels are estimated. Empirical experiments showed that a 6° spline was the simplest model of the profile, that can take different left and right background levels into account and suppress the influence of the presence of a possible AR. Higher order splines showed to model a possible AR which we need to avoid in the following scheme. Fig. 4 shows a typical profile overlaid a smoothing cubic spline S of 6° of freedom. It also shows the first and second derivatives of the spline (S' and S''). In general, the smoothed profile's derivatives show the characteristics as seen in the figure: S' has a local minimum to the left of the centre and a local maximum to the right of the centre. S'' has local minima further away from the centre, than the local extrema in S'. The positions of these minima are used as estimates of the location of the background levels. This knowledge of the general shape of the profile's derivatives leads to important information, necessary to obtain robust estimates of the background intensities on each side of the vessel. The procedure is as follows.

- Find global minimiser, $P_{\min}$ of the profile P around the centre of the profile, i.e., in the interval [*centre–midzone*; *centre* + *midzone*], where *centre* is the centre pixel in the profile and *midzone* is an adjustable parameter. In the present application *midzone* equals 1/6 of the entire profile width. In Fig. 4(a), the minimiser is referred to as $P_{\min}$.
- Search for a global minimiser of S' to the left of $P_{\min}$. We call this minimiser $S'_{\min}$.
- Search for a global maximiser of S' to the right of $P_{\min}$. This is $S'_{\max}$. $S'_{\min}$ and $S'_{\max}$ are indicated in Fig. 4(b).
- Find first local minimiser of S'' to the left of $S'_{\min}$. This is S''_{LeftMin}. First means closest to centre, $P_{\min}$.
- Similarly, find first local minimiser of S'' to the right of $S'_{\max}$. This minimiser is denoted S''_{RightMin}.
- Estimates of the background intensity levels can be calculated as the mean values of P in the vicinity of S''_{LeftMin} and S''_{RightMin}. The vicinity range is 5% of the distance between S''_{LeftMin} and S''_{RightMin} and is centered around S''_{LeftMin} and S''_{RightMin}, respectively. The S'' minimisers are shown both in Figs. 4(a) and (c).

2.3.2. Full width half maximum

A typical intensity profile orthogonal to a retinal vessel is shaped similar to a Gaussian curve. Here although, low image intensity corresponds to low pixel value and therefore, we try to estimate the full-width at half-*minimum*, but the methods are analogue. Fig. 5 illustrates the principles. Here, two distinct minima levels (*MinLeftLevel* and *MinRightLevel*) are used due to the presence of an AR. The half minimum in the left side is calculated as the mean of the left background level (*MaxLeftLevel*) and the left minimum level (*MinLeftLevel*). The half minimum in the right side is vice versa. The FWHM estimate of the profile width,

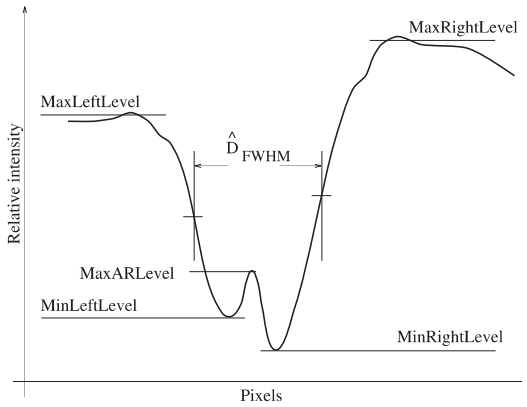

Fig. 5. Principles of full width half minimum estimation of vessel width. The estimated profile width, $\hat{D}_{FWHM}$ is the distance between the two vertical dashed lines.

$\hat{D}_{FWHM}$ is then the *full width* between the two half minima. Note, that this method is not sensitive to the presence of an AR or to different background levels (*MaxLeftLevel* and *MaxRightLevel*).

The FWHM method used to assess retinal vessel diameters is described in further in detail (Brinchmann-Hansen and Heier, 1986).

The algorithm in Section 2.3.1 has been extended to find an AR. Between the edges found using the FWHM method, a new smoothing spline is fitted to the profile. The number of extrema in this range is used to determine the presence of an AR.

The example images in Fig. 6 show the results of the FWHM vessel diameter measurement.

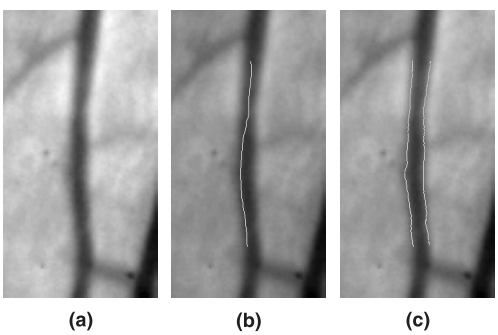

Fig. 6. Trace and edges found in example vessel segment. (a) – Example of arterial vessel segment; (b) – (a) with shortest path overlaid and (c) – (a) with the FWHM edges overlaid.

2.3.3. Alternative diameter measurement

Gregson et al. (1995) have proposed an alternative method to measure the width of an intensity profile. In this method it is assumed, that the intensity profile can be modelled with a rectangular profile. A rectangular profile of a fixed height is then fitted to the profile data. The principles are shown in Fig. 7. The height of the rectangle is $MaxLevel - MinLevel$. The width of the rectangle, $\hat{D}_{Gregson}$ is adjusted until the area (in the window, W) under the rectangular model is equal to the area under the actual intensity profile. See Gregson et al. (1995) and Kozousek et al. (1992) for further details.

2.4. Focal arteriolar narrowing measurement

The width (also referred to as the calibre or the diameter) of a *normal* vessel is expected to decrease monotonously as the distance from the *papilla* increases. Between bifurcations, the normal diameter should be constant or slightly decreasing due to small bifurcations (branches) not visible by the naked eye. Fig. 8 illustrates the course of a normal vessel and a vessel width (exaggerated) FAN.

With the purpose of detecting changes in the vessel diameter we calculate two features, the coefficient of variance (CV) of the vessel diameter and the normalised accumulated gradient (NAG).

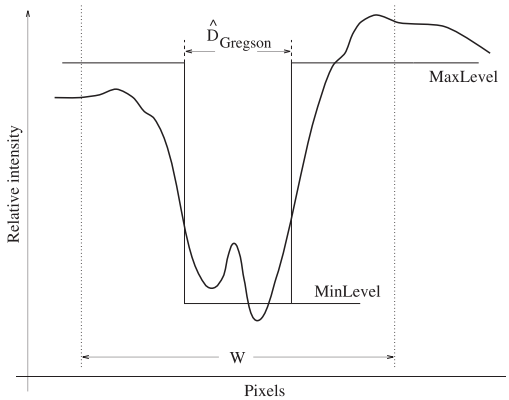

Fig. 7. Principles of Gregson's method for vessel width assessment. $\hat{D}_{Gregson}$ is the estimate of the vessel width.

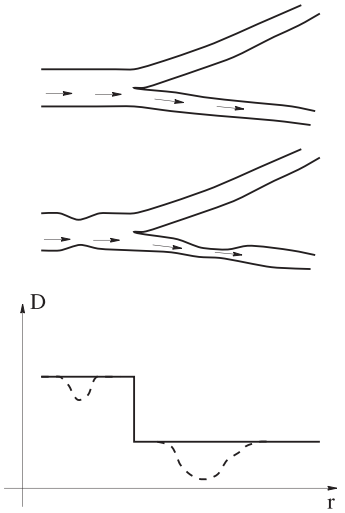

Fig. 8. The vessel diameter D as a function of the distance r to the *papilla*. As the vessel branches, the diameter drops instantly. Top: normal vessel; Middle: vessel with FAN; Bottom: vessel diameters in the lower branch. Solid line is normal, dashed line shows FAN.

For both features, large values correspond to a high degree of FAN. By definition, the CV is the standard deviation divided by the mean value. The NAG is described in Section 2.4.1.

2.4.1. Normalised accumulated gradient

A focal narrowing consists of a decrease followed by an increase in the vessel diameter (see Fig. 1). Because an over-seen bifurcation may result in a *decrease* in the vessel diameter, a decrease alone is *not* enough to indicate a focal narrowing.

However, if the diameter *increases*, this must be due to a focal narrowing. We therefore, aim to detect *increments* in the vessel diameter as the distance to the *papilla increases*. This corresponds to situations where the gradient of the diameter is positive. The idea is illustrated in Fig. 9.

Let φ be the function

$$\varphi(x) = \begin{cases} 1 & \text{if} \quad x > 0, \\ 0 & \text{else}, \end{cases} \tag{3}$$

with ∇ as the difference operator and with $\underline{\hat{D}}_i$ as the estimated vessel diameter in point i,

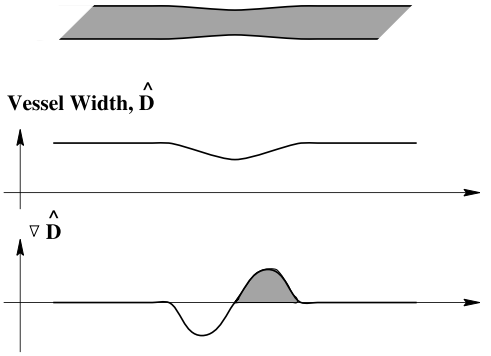

Fig. 9. Principle of normalised accumulated gradient (NAG). Top: vessel with focal arteriolar narrowing (FAN); Middle: diameter of vessel; Bottom: first derivative of vessel diameter. The shaded area in the bottom figure corresponds to the NAG.

$$\nabla \underline{\hat{D}}_i = \begin{bmatrix} \hat{D}_{i,2} - \hat{D}_{i,1} \\ \vdots \\ \hat{D}_{i,m_i} - \hat{D}_{i,m_i-1} \end{bmatrix}, \tag{4}$$

is an approximation to the gradient of $\underline{\hat{D}}_i$. The NAG is then defined as

$$NAG_i = \frac{1}{m_i E(\underline{\hat{D}}_i)} (\nabla \underline{\hat{D}}_i)^T \varphi(\nabla \underline{\hat{D}}_i), \tag{5}$$

i.e., the sum of the squared *positive* parts of the gradient of $\underline{\hat{D}}_i$ normalised with respect to the mean vessel segment diameter and the number of profiles, m_i in the vessel segment.

3. Comparative FAN measurement study

A comparative study between a skilled ophthalmologist and the image analysis based methods has been conducted. We hereby, aim to investigate if the developed methods are able to predict the FAN status of vessel segments as assessed by the ophthalmologist.

Since branch retinal vein occlusion (BRVO) is known to be strongly associated with risk factors for hypertension and arteriosclerosis, BRVO patients were used as a prototype study group with macro-vascular disease that was compared with a background population without any predilection for macro-vascular disease.

3.1. Material

The fundus images in this work were captured directly, in "red-free" light using a CCD fundus camera. The fundus camera used is a Topcon TRC-50X Retina Camera, equipped with a Kodak MegaPlus model 1.4 digital backpiece. The images were handled using a PC-based image handling system (Ophthalmic Imaging Systems, Sacramento, CA, USA). The resolution is 1024×1024 in eight-bit grey scale. Since the data is captured directly there is no film developing or digitizing process. The data is stored in an uncompressed tiff format. The "red-free" light is suitable for visualisation of the blood vessels in the retina and agrees with the recommendations in (Delori et al., 1977).

298 arterial vessel segments without bifurcations or arterio–venous (A/V) crossings were extracted from the fundus images of 30 subjects (15 from the background population and 15 with unilateral BRVO). The images of the patients with unilateral BRVO were captured of the "healthy" eye, i.e., the eye without BRVO. The segments were then, after a random permutation, shown individually to an ophthalmologist. The clinician answered the question "Is FAN present in the segment?" with one of three possible answers: "yes", "cannot be assessed" or "no" corresponding to the values "+", "NA" and "−", respectively. The rating of the individual segments was performed *twice* on the same day.

3.2. Ophthalmologist's experimental ratings

Table 1 shows the results of the two ratings.

The evaluation of the vessel segments is consistent in 199 (the sum of the diagonal elements) of 298 segments and the ratings are highly inconsistent in 10 $(7 + 3)$ cases.

The accuracy or proportion of agreement (Bradley, 1997) is 67%. Leaving out the 99 segments, where the ophthalmologist were not able to assess the FAN status in at least one of the ratings, the reproducibility is $(75 + 86)/(75 + 86 + 3 + 10) = 94\%$.

Table 1
Association between two ratings by the ophthalmologist on 298 individual arteriolar vessel segments. "+" corresponds to "yes, FAN is present", "NA" to "cannot be assessed" and "−" to "no signs of FAN"

	Second rating			Total
	−	NA	+	
First rating				
−	86	14	3	103
NA	36	38	20	94
+	7	19	75	101
Total	129	71	108	298

A κ-analysis showed that in both cases the ophthalmologist was significantly better, at all levels, than random choice.

3.3. Image analysis FAN classification results

To obtain a set of vessel segments with highly reliable FAN status as "ground truth", we used only the segments with *consistent and distinct* ophthalmologist evaluation in the comparison with the developed FAN measurement method, i.e., $86 + 75 = 161$ segments were considered. The FAN measurements (CV and NAG) were calculated using both the FWHM method and the Gregson method for diameter measurement. A classification threshold is computed which minimises the sum of the fractions of missed positive ("+") cases and missed negative ("−") cases. Using resubstitution, test sample and ordinary cross validation the accuracy results in Table 2 are obtained. The accuracy values correspond to the degree of match between the developed methods and the evaluation by the ophthalmologist.

From the accuracy results in Table 2, we see that the CV feature calculated using FWHM based diameter measurements has the best match to the ophthalmologist's FAN evaluation. For two classification methods this feature comes to the same result as the ophthalmologist in at least 80% of the segments. This indicates that this feature is able to estimate the FAN in vessel segments.

The NAG feature performs best in combination with the Gregson based diameter measurements.

Table 2
Accuracy results of resubstitution, test sample, and cross validation classifications for the CV and the normalised accumulated gradient (NAG) estimation of the degree of focal arteriolar narrowing (FAN). The accuracies show the degree of agreement with the ophthalmologist

	CV		NAG	
	FWHM	Gregson	FWHM	Gregson
Resubstitution	0.82	0.73	0.72	0.74
Test sample	0.81	0.74	0.60	0.74
Cross validation	0.74	0.72	0.70	0.74

We here obtain accuracies of 74%, i.e., the method classifies 74% of the segments in agreement with the ophthalmologist FAN evaluation.

In general, the CV feature seems to match the ophthalmologist's opinion better than the NAG feature does. In addition, the FWHM seems to be the more reliable method for vessel diameter assessment.

4. Summary and conclusion

In this work, we have aimed to develop a method to quantify the changes in retinal vessel diameters from images of the human retina (fundus images). More specifically, to objectively assess the focal arteriolar narrowing (FAN) status of arteriolar vessel segments. We have investigated the performance of two methods to measure retinal vessel diameters in ocular fundus images. Furthermore, two methods for quantification of FAN have been proposed and tested on 161 arteriolar vessel segments from 30 subjects.

From the results of the quantitative image analysis, we conclude that the developed methods to some extent are able to detect FAN in retinal arteriole segments at a level, comparable to the level of an ophthalmologist. It seems, that the full width half maximum estimation of the vessel diameter in combination with the (simple) CV statistic has the best match to the ophthalmologist evaluations of FAN in the vessel segments considered. We can also conclude that the more sophisticated NAG statistic is not as well performing on the considered data set as the CV statistic. However, we still believe that the NAG statistic provides useful information about the condition of the vessels.

Current clinical standards of describing retinal arteriolar changes secondary to arterial hypertension and/or arteriosclerosis is limited to two levels of abnormality, fundus hypertonicus I and II. We believe that quantitative image analysis holds a potential for a finer non-invasive grading of such pathological vascular changes.

Acknowledgements

Torsana Diabetes Diagnostics A/S, Denmark financially supported this study. Department of Ophthalmology, Herlev Hospital, University of Copenhagen is acknowledged for selecting and providing the image material.

References

Albert, D.M., Jakobiec, F.A., 1994. Principles and Practice of Ophthalmology. W.B. Saunders Company, Philadelphia.

Bradley, A.P., 1997. The use of the area under the curve in the evaluation of machine learning algorithms. Pattern Recognition 30 (7), 1145–1159.

Brinchmann-Hansen, O., Engvold, O., 1986. Microphotometry of the blood column and the light streak on retinal vessels in fundus photographs. Acta Ophthalmolog. Suppl. 179, 9–19.

Brinchmann-Hansen, O., Heier, H., 1986. The apparent and true width of the blood column in retinal vessels. Acta Ophthalmolog. Suppl. 179, 29–32.

Brinchmann-Hansen, O., Heier, H., 1986. Theoretical relations between light streak characteristics and optical properties of retinal vessels. Acta Ophthalmolog. Suppl. 179, 33–37.

Cormen, T.H., Leiserson, C.E., Rivest, R.L., 1997. Introduction to Algorithms. In: The MIT Electrical Engineering and Computer Science Series. The MIT Press, Cambridge, MA.

Delori, F.C., Gragoudas, E.S., Francisco, R., Pruett, R.C., 1977. Monochromatic Ophthalmoscopy and Fundus Photography. The Normal Fundus. Arch Ophthalmol. 95, 861–868.

Dijkstra, E.W., 1959. A note on two problems in connexion with graphs. Numerische Mathematik 1, 269–271.

Early Treatment Diabetic Retinopathy Study Group 1992. Fundus photographic risk factors for progression of diabetic retinopathy. ETDRS Rep. No. 12. Ophthalmology 98, 823–833.

Gregson, P.H., Shen, Z., Scott, R.C., Kozousek, V., 1995. Automated Grading of Venous Beading. Comput. and Biomed. Res. 28, 291–304.

Kozousek, V., Shen, Z., Gregson, P., Scott, R.C., 1992. Automated detection and quantification of venous beading using Fourier analysis. Can. J. Ophthalmolog. 27 (6), 288–294.